PCCP

RSC Publishing

COMMUNICATION

View Article Online
View Journal

Solution-processed small molecule:fullerene bulk-heterojunction solar cells: impedance spectroscopy deduced bulk and interfacial limits to fill-factors†

Cite this: DOI: 10.1039/c3cp52363b

Received 24th June 2013,
Accepted 23rd July 2013

DOI: 10.1039/c3cp52363b

www.rsc.org/pccp

Antonio Guerrero,‡[a] Stephen Loser,‡[b] Germà Garcia-Belmonte,[a] Carson J. Bruns,[cd] Jeremy Smith,[b] Hiroyuki Miyauchi,[b] Samuel I. Stupp,[cd] Juan Bisquert*[a] and Tobin J. Marks*[b]

Using impedance spectroscopy, we demonstrate that the low fill factor (FF) typically observed in small molecule solar cells is due to hindered carrier transport through the active layer and hindered charge transfer through the anode interfacial layer (IFL). By carefully tuning the active layer thickness and anode IFL in BDT(TDPP)$_2$ solar cells, the FF is increased from 33 to 55% and the PCE from 1.9 to 3.8%. These results underscore the importance of simultaneously optimizing active layer thickness and IFL in small molecule solar cells.

1. Introduction

Rapid material developments in bulk-heterojunction (BHJ) organic photovoltaic (OPV) research have led to impressive performance advances, with confirmed power conversion efficiencies (PCEs) now reaching ~10%.[1] In BHJ cells, interpenetrating networks of donor and acceptor molecules/macromolecules harvest sunlight and generate charge carriers that are collected at selective electrodes.[2] Most research to date has focused on polymeric donors and fullerene molecular acceptors.[3,4] Recent progress in solution-processed small donor molecule BHJ OPVs, however, has highlighted the potential to overcome many of the synthetic and processing challenges associated with polymeric donors.[5–18] Nevertheless, for the majority of small molecule donor OPVs, conspicuously low fill factors (FFs) are observed, and further mechanistic understanding will be required to improve efficiencies. In this contribution, we seek better understanding of why devices fabricated with small molecule donors typically exhibit lower FFs than their polymeric analogues and how this disparity might be rectified.

The approach here is to understand these differences by comparing the properties of OPVs fabricated with the well-studied polymeric donor–acceptor system poly(3-hexylthiophene) (**P3HT**):$PC_{61}BM$, which consistently yields FFs $\geq$ 65%,[19] with a small molecule donor–acceptor system that typically provides low FFs. Using impedance spectroscopy (IS) we identify additional resistances for the small molecule system which are not observed in the polymer system. We show that these additional resistive effects severely limit FFs in the small molecule OPVs and arise from losses related to *both* charge transport within the active layer blend and charge transfer from the active layer to the anode interfacial layer (IFL). By careful optimization of the active layer thickness and anode IFL, we demonstrate that the additional resistances in the impedance spectra can be significantly suppressed and device performance significantly enhanced. We show that the impedance spectroscopy analysis can also be applied to other higher efficiency small molecule systems.

2. Results and discussion

This study utilizes a new small molecule donor BDT(TDPP)$_2$-6,6′-(5,5′-(4,8-bis((2-ethylhexyl)oxy)benzo[1,2-*b*:4,5-*b*′]dithiophene-2,6-diyl)bis(thiophene-5,2-diyl))bis(2,5-bis(2-ethylhexyl)-3-(thiophen-2-yl)pyrrolo[3,4-*c*]pyrrole-4(2*H*,5*H*)-dione) abbreviated as **BDT** (Fig. 1; see ESI† for the synthesis). Previous results showed that fused acene small molecule cores flanked by thiophene-capped diketopyrrolopyrrole (TDPP) units provide excellent light capture and high ionization potentials (IPs), thus yielding excellent OPV short circuit current densities (J_{sc}) and open circuit voltages (V_{oc}) similar to those reported previously for **z-NDT**(TDPP)$_2$ (Fig. 1).[20,21]

[a] *Photovoltaic and Optoelectronic Devices Group, Departament de Física, Universitat Jaume I, ES-12071 Castelló, Spain. E-mail: bisquert@uji.es*
[b] *Department of Chemistry and the Argonne-Northwestern Solar Energy Research (ANSER) Center, Northwestern University, 2145 Sheridan Road, Evanston, IL 60208, USA. E-mail: t-marks@northwestern.edu; Tel: +1 847-491-5652*
[c] *Department of Chemistry, Department of Materials Science and Engineering, Northwestern University, Evanston, Illinois 60208, USA*
[d] *Department of Medicine and the Institute for BioNanotechnology in Medicine, Northwestern University, Chicago, Illinois 60611, USA*

† Electronic supplementary information (ESI) available: Full experimental and synthetic details, electrochemical and optical properties of films, device optimization, and AFM micrographs of active layer blends. See DOI: 10.1039/c3cp52363b

‡ These authors contributed equally.

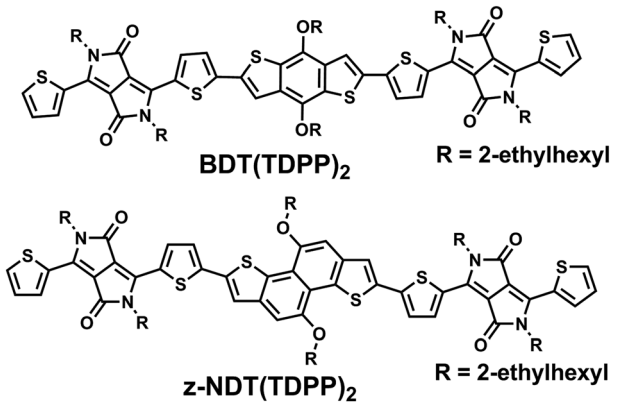

Fig. 1 Molecular structure of the small molecule donors **BDT**(TDPP)$_2$ and **z-NDT**(TDPP)$_2$.

Optimized **BDT**:$PC_{61}BM$ OPVs having the architecture ITO/PEDOT:PSS/active layer/Ca/Ag afford the performance parameters J_{sc} = 10.0 mA cm^{-2} and V_{oc} = 0.81 V, which are significantly greater than those of an optimized **P3HT**:$PC_{61}BM$ OPV (Fig. 2a; Table 1 entries 1 and 2). Strikingly, however, the **P3HT** device FF is significantly greater (67%) than that of the **BDT** device (37%), which is similar to that of most solution-processed small molecule OPVs.[7] The reasons can be partly understood from microstructural and hole mobility analysis.[8] Next, AFM analysis is carried out on the **P3HT**:$PC_{61}BM$ and **BDT**:$PC_{61}BM$ films (Fig. S4, ESI†). Compared to the small molecule system, the **P3HT**:$PC_{61}BM$ films have larger domains with more fibrillar regions, suggesting better electrical connectivity. Interestingly, comparing the AFM images of a recently reported high efficiency (7.38%) small molecule device[18] with those reported for **BDT**:$PC_{61}BM$ shows them to be rather similar, indicating that microcrystallinity alone, as inferred from AFM images, is insufficient to account for the lower FF. It will be seen here that impedance spectroscopy (IS) reveals that the small molecule TDPP system is indeed limited by carrier transport.

To shed more light on the origin of the low small molecule FFs, an impedance spectroscopy (IS) analysis was carried out on the **P3HT**:$PC_{61}BM$ and **BDT**:$PC_{61}BM$ OPVs. IS techniques have proven to be powerful tools for quantifying OPV recombination rates.[22,23] Here, a small AC voltage perturbation is applied at varying DC voltage biases and the differential current output measured. The AC voltage frequency is then varied to analyze the differential current response, with the measurements carried out as a function of DC voltage to encompass the entire OPV operating regime.

IS spectra of the **P3HT**:$PC_{61}BM$ and **BDT**:$PC_{61}BM$ OPVs are compared in Fig. 2b and c (devices 1 and 2). There is a striking difference in the spectra, which will be shown to correlate with the large differences in device FF. The methods for OPV IS measurement interpretation have been explained in a number of review and research papers. Here we only briefly summarize the significance of key parameters and refer the reader to the previous papers for a full account of the interpretation tools.[24–26]

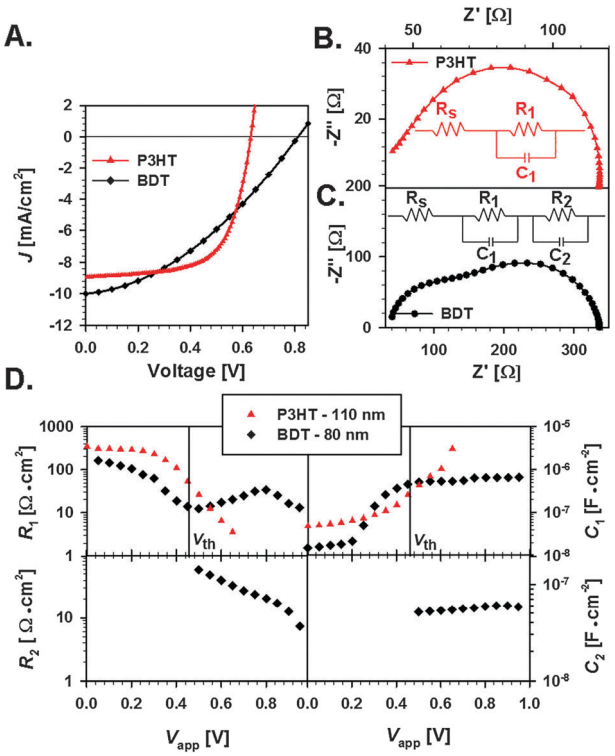

Fig. 2 (a) *J–V* response of OPV devices using the standard architecture: ITO/PEDOT:PSS/active layer/Ca/Ag. Impedance response measured at 1 sun illumination and equivalent circuit model used for systems not limited by transport effects such as **P3HT**:$PC_{61}BM$ (b), and for systems limited by carrier transport such as **BDT**:$PC_{61}BM$ (c). (d) Fitting results for the same devices. V_{th} indicates the approximate threshold at which R_1 changes tendency.

Table 1 OPV device performance parameters

Entry	Donor molecule	IFL	J_{SC} [mA cm^{-2}]	V_{oc} [V]	FF [%]	PCE [%]
1	**P3HT**[a]	PEDOT:PSS	8.9	0.62	67	3.7
2	**BDT**[b]	PEDOT:PSS	10.0	0.81	37	3.0
3	**BDT**[c]	PEDOT:PSS	7.6	0.84	49	3.1
4	**BDT**[d]	PEDOT:PSS	8.2	0.84	42	2.9
5	**BDT**[e]	PEDOT:PSS	5.5	0.82	32	1.5
6	**BDT**[f]	PEDOT:PSS[j]	7.4	0.78	33	1.9
7	**BDT**[g]	MoO_3	7.6	0.85	55	3.5
8	**BDT**[h]	MoO_3	8.7	0.85	51	3.8
9	**z-NDT**[i]	PEDOT:PSS[j]	11.9	0.76	48	4.3

Active layer thickness: [a] 110 nm. [b] 80 nm. [c] 45 nm. [d] 65 nm. [e] 110 nm. [f] 45 nm. [g] 45 nm. [h] 50 nm. [i] 80 nm. [j] Air-dried.

In many cases it has been observed that when doping an organic blend (donor density N_D), so that it contains a stable population of majority electronic carriers (holes in the donor material) of density $p = N_D$, the open circuit voltage is associated with the rise of the minority carrier Fermi level (electrons in the fullerene), and is determined by the recombination flux (J_{rec}). These features provide a simple IS model consisting of the parallel combination of recombination resistance R_{rec} and chemical capacitance C_μ. The capacitance C_μ indexes the ability

of the system to store minority carriers (electrons)[25] due to the rise of the electron Fermi level in the fullerene phase. It has been shown that when E_{Fn} is deliberately displaced, the chemical capacitance provides an accurate measure of the density of states (DOS) on the fullerene.[24] On the other hand, the *recombination resistance* is defined as[22,23]

$$R_{rec} = \left(\frac{\partial J_{rec}}{\partial V_F}\right)^{-1} \quad (1)$$

The recombination flux J_{rec} can then be expressed in terms of the density of minority carrier electrons, n, as

$$J_{rec} = qLk_{rec}n^{\beta} \quad (2)$$

where q is the elementary charge, L is the film thickness, and k_{rec} is a constant. In a solar cell controlled only by recombination which does not exhibit transport or series resistance limitations, using the Boltzmann statistics (k_BT is thermal energy) in eqn (2) we can write the diode model as follows:

$$j = j_0\left[\exp\left(\beta\frac{V_F}{k_BT/q}\right) - 1\right] - j_{ph} \quad (3)$$

where j_0 stands for the saturation current and j_{ph} accounts for the photocurrent. The parameter β represents an effective recombination order that directly translates into the diode quality factor, and therefore determines the shape of the diode curve and the FF. Additionally other factors may limit the solar cell performance, and they appear as additional resistances that *decrease* the fill factor and eventually the photocurrent. The *total resistance* measured by IS is related to the derivative of the *J–V* plot (at any voltage) as,

$$R_{tot} = \left(\frac{\partial J}{\partial V}\right)^{-1} \quad (4)$$

In IS analysis the resistance R_{rec} can be separated from other resistive contributions. For the model of eqn (2) we have,

$$R_{rec} = R_{rec,0}\exp\left(-\frac{q\beta V_F}{k_BT}\right) \quad (5)$$

The voltage V_F represents the rise in the electron Fermi level, and is derived by subtracting the series potential drop from the applied voltage, V_{app}.

The characteristic features of the simple impedance model are often observed in the **P3HT**:$PC_{61}BM$ devices.[24] Accordingly the IS response of this device shows a single arc (Fig. 2c), which can be interpreted in terms of R_{rec} and C_μ which correspond to elements R_1 and C_1 in the equivalent circuit shown in Fig. 2b (inset). The behaviour of R_1 for the **P3HT**:$PC_{61}BM$ device (Fig. 2d) indicates an exponential decrease with the voltage between 0.3 V and V_{oc}, and can be attributed to R_{rec} as shown in eqn (5).[22,23] This interpretation of the **P3HT**:$PC_{61}BM$ device data is further corroborated by the behaviour of the capacitance C_1, which increases exponentially with voltage as a standard chemical capacitance.[24]

In contrast to this standard behaviour, the **BDT**:$PC_{61}BM$ OPV shows an additional feature that consists of a second arc at high frequency, Fig. 2c. The circuit required to fit these small molecule impedance spectra consists of two additional elements R_2 and C_2 (Fig. 2c, inset). Assuming that the low frequency resistor R_1 can be interpreted as R_{rec} and defines the diode shape, the high frequency resistor R_2 represents an absolute loss of the photogenerated power. According to eqn (2) the additional R_2 increases the reciprocal of $\partial J/\partial V$ and therefore flattens the *J–V* curve and depresses the FF, as discussed above. R_{tot} also includes a series resistance, R_s, corresponding to the high frequency intercept of the IS spectrum, which arises from the contacts and substrates.

In a more detailed analysis, it can be seen in Fig. 2d that for **BDT**:$PC_{61}BM$, R_1 does decrease exponentially as R_{rec}, but only up to a certain voltage which is denoted here as the threshold voltage (V_{th}). Thereafter, R_1 *increases* with voltage instead of the expected decrease. This feature is accompanied by a leveling off of C_μ, indicating that the electron Fermi level no longer spans the DOS of the fullerene, *i.e.*, E_{Fn} does not rise into the bandgap despite the voltage increase. This is a direct consequence of the presence of two electrical processes connected in series in which recombination is dominant at low applied voltages and interfacial charge transfer at high applied voltages. Thus, understanding the physical origin of both resistances R_1 and R_2 that severely limit the PCE of **BDT**:$PC_{61}BM$ OPVs is essential.

To this end, in the next stage of the investigation, the active layer thickness of the **BDT**-based devices was systematically varied from 40 nm to 110 nm, using a PEDOT:PSS IFL as the standard contact. The results for the three cells are shown in Fig. 3 (devices 3–5). The principal aim of changing the active layer thickness is to distinguish, in the IS spectra, between physical phenomena occurring in the bulk blend which depend

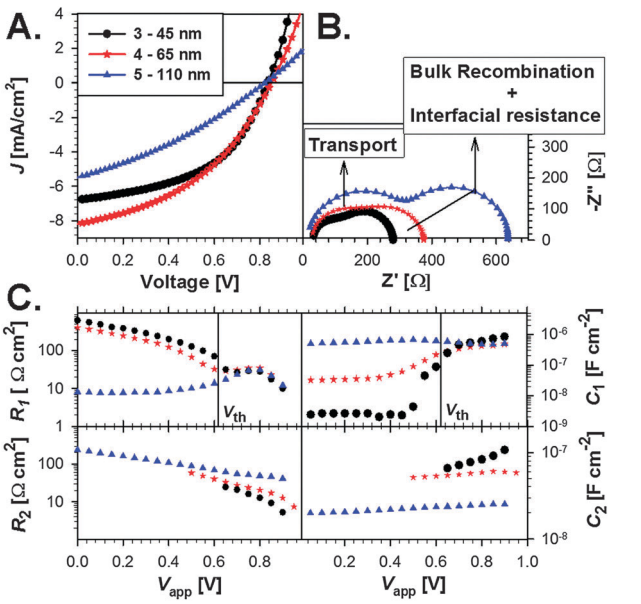

Fig. 3 (a) *J–V* response of small molecule donor OPVs using the standard device architecture: ITO/IFL/**BDT**:$PC_{61}BM$/Ca/Ag. The effect of active layer thickness is studied with IFL = PEDOT:PSS dried under N_2. (b) Impedance spectra of devices shown in (a) measured at 1 sun illumination at V_{oc}. (c) Fitting results for the same devices. V_{th} indicates the approximate threshold at which R_1 changes tendency.

on volume, and those occurring at the macroscopic contacts. For example, the total rate of recombination in organic BHJ blends depends on volume and should scale with thickness. Reducing the active layer thickness should suppress recombination, and therefore enhance V_{oc}, if the total generation rate is the same.[27–30] On the other hand, light absorption and carrier generation, which determine J_{sc}, should increase with thickness. Indeed the J_{sc} of the 65 nm **BDT**:$PC_{61}BM$ device is greater than that of the device with an active layer thickness of 45 nm. However, a further increase in active layer thickness to 110 nm leads to reduced charge collection, and a very low quality device. An important fact evident in Fig. 3a is that V_{oc} is *invariant* across the series of active layer thicknesses. A related behaviour, in which V_{oc} is nearly invariant with respect to the illumination level, was reported by Zhang *et al.*[31] for a similar type of device. The *J–V* response also reveals that the device with the thinnest active layer has the highest FF, which noticeably falls with increasing active layer thickness (Table 1, entries 3–5).

Deeper insight into these features in the **BDT**:$PC_{61}BM$ *J–V* curves comes from interpreting the impedance results. A clear correlation between the active layer thickness and the resistance of the high frequency arc (R_2) is evident (Fig. 3b and c). The **BDT**:$PC_{61}BM$ device with the *thinnest* active layer exhibits the *smallest* resistance R_2 (10–30 Ω cm^2) and this resistance scales with the active layer thickness, *i.e.* 100 Ω cm^2 for the thickest cell (entry 5). Additionally, the capacitance associated with this arc falls as the active layer thicknesses are increased, which is expected from the dielectric capacitance associated with the film geometric capacitance.[25] This thickness dependence indicates that R_2 can be ascribed to a transport resistance (R_{tr}).[32] Since this resistance is coupled to the geometric capacitance (and not to the chemical capacitance as previously shown for systems based on **P3HT**:$PC_{61}BM$), we assume that the R_{tr} is related to majority carriers (holes).[11] Note that well-separated IS arcs over the entire operating voltage range are only observed for cells having an active layer thickness of 110 nm. As the active layer thickness is decreased, the voltage at which the two arcs are observed increases. Note also that the presence of a high frequency arc was recently observed by IS in polymer-based OPVs when carrier transport was deliberatively reduced by introducing traps.[33] The thinnest active layer exhibits the smallest, least defined additional arc, thus connecting active layer thickness and bulk active layer charge transport with device FF. The results in Fig. 3 show that when the active layer thickness is reduced to 40 nm, the loss in PCE resulting from the FF is greatly suppressed, and FFs of 49% are achievable – significantly higher than the 32% measured for the 110 nm active layer OPV.

Concerning the resistance of the low frequency arc, which is connected with the recombination resistance that exists in all solar cells, as indicated in eqn (1), Fig. 3c shows the same behaviour identified in Fig. 2 for the three different thickness devices: below the threshold voltage V_{th}, R_1 decreases with increasing voltage as is typical for R_{rec} and, as expected, this resistance scales with thickness. R_{rec} can be analyzed in terms of the effective recombination order (β) that is connected with the diode quality and determines the shape of the *J–V* curve, as indicated in eqn (2) and (5).[34] High values of β provide high FFs. In good agreement with this rule, values of β calculated for **P3HT**:$PC_{61}BM$ from eqn (5) show the highest β value obtained in this work (β = 0.51, FF = 67%), the lowest recombination rates, and the highest FF. On the other hand, β values for the **BDT**:$PC_{61}BM$ system are smaller, indicating higher recombination rates and lower FFs than those of the polymeric analogue. See for example, Table 1 entries 3 (β = 0.40, FF = 49%) and 4 (β = 0.35, FF = 42%).

At a threshold voltage V_{th}, the R_1 parameter becomes completely pinned. Fig. 3c also shows clearly that both V_{th} and the value of R_1 at $V > V_{th}$ are independent of thickness. This result strongly links this pinned resistance with the macroscopic contact since the electrical response of processes occurring in the bulk of the active layer would depend on its thickness.

To further investigate the impedance spectroscopic features with the overall goal of enhancing small molecule OPV FFs, the anode IFL was varied. IFLs have been recently implemented to adjust OPV energy level alignment, enhance physical cohesion, and block minority carrier leakage at the active layer-anode interface, thereby significantly enhancing PCE and durability.[35–37] Nevertheless, a recent small molecule OPV review indicates that this strategy has barely influenced the field.[7] Analysis of data reviewed by Mishra *et al.* shows that of over 100 different small molecule donors that have been investigated in OPVs (average FF = 39%), only six were examined with a non-PEDOT:PSS IFL.

An effective OPV IFL must ensure good energy level matching with the appropriate charge carriers, *e.g.*, the electron affinity (EA) of the electron transporting material with the cathode IFL,[38,39] and the IP of the hole transporting material with the anode IFL.[40–43] By cyclic voltammetry, the **BDT** IP is found to be large, 5.5 eV, whereas the **P3HT** IP lies at 5.2 eV (see ESI†). These values can be used, as an approximation, to provide information on the energy level alignment of the active layer and the anode as shown in Fig. 4. Thus, the optimal anode IFL (PEDOT:PSS) for **P3HT** is unlikely to be optimum for **BDT** due to energetic mismatches, and such mismatches are probably the origin of the increased resistances of the low frequency arc as V_{oc} is approached in **BDT**:$PC_{61}BM$ OPVs. To this end, the

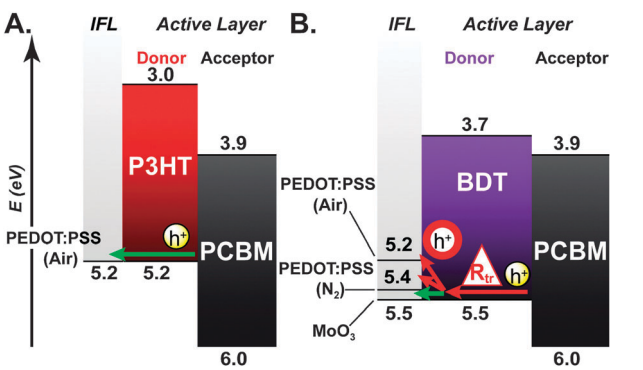

Fig. 4 Energy level diagram showing the materials studied in this work and an estimation of the energy level match–mismatch between the hole transporting active material and the IFL.

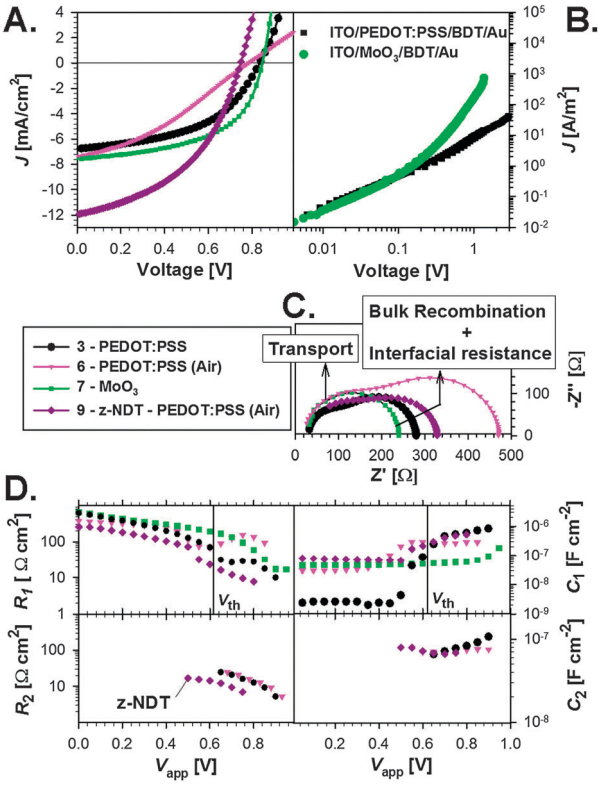

Fig. 5 (a) *J–V* response of small molecule donor OPVs using the standard device architecture: ITO/IFL/**BDT**:$PC_{61}BM$/Ca/Ag. The IFL anode is modified to test the importance of the energy level matching at the active layer/anode interface; the IFLs are air-dried PEDOT:PSS and thermally evaporated MoO_3 exposed to air. Device 9 is based on a higher efficiency small molecule donor (**z-NDT**) in the configuration ITO/PEDOT:PSS/**z-NDT**:$PC_{61}BM$/Ca/Ag, (b) *J–V* response of hole only-diodes based on the architecture: ITO/IFL/**BDT** (50 nm)/Au, where the IFL is either MoO_3 (5 nm) or PEDOT:PSS (dried in the glovebox). (c) Impedance spectra of devices shown in (a) measured at 1 sun illumination at V_{oc}. (d) Fitting results for the same devices. V_{th} indicates the approximate threshold at which R_1 changes tendency.

optimized **BDT**:$PC_{61}BM$ active layer film thickness (~40 nm) was investigated with three different IFL materials, Fig. 5, all having distinctly different WFs: PEDOT:PSS dried in air (5.2 eV),[44] already discussed PEDOT:PSS dried under N_2 (5.4 eV),[44] and thermally evaporated MoO_3 exposed to air (5.5 eV).[45,46]

Using the air-dried PEDOT:PSS IFL, the **BDT** OPV *J–V* plot clearly exhibits a dramatically reduced FF and lower photovoltage compared to PEDOT:PSS dried in the glovebox, while J_{sc} is unchanged (Fig. 5a and Table 1, entries 3, 6 and 7). The thermally evaporated MoO_3 IFL thickness was then optimized, and optimum results were obtained from a 5 nm thick film (Table 1, entry 7; see ESI† for details). The optimized devices show J_{sc} and V_{oc} values comparable to those of the PEDOT:PSS glovebox-dried OPV. However, more importantly, the FF is significantly enhanced for all MoO_3-based devices – up to a 67% increase *versus* the air-dried PEDOT:PSS IFL and a 15% increase *versus* the glovebox-dried PEDOT:PSS IFL. Upon optimizing the active layer thickness, PCE = 3.8% is achieved using the 5 nm MoO_3 IFL (entry 8). Note that regardless of the IFL used, the **BDT**:$PC_{61}BM$ active layer morphology appears to be identical on each substrate (Fig. S4 and S5, ESI†), as revealed by AFM and XRD analysis, which confirms that the morphology of the active layer is neither affected by the IFL choice, nor does the morphology influence the large observed enhancement in FF when changing from an air-dried PEDOT:PSS IFL to a MoO_3 IFL.

Additionally, *J–V* curves corresponding to hole-only diodes (see Fig. 5b) constructed in the architecture ITO/IFL/**BDT**/Au, where the IFL is either PEDOT:PSS (glovebox dried) or MoO_3, confirm that the MoO_3 has superior hole-transfer properties than PEDOT:PSS. Hole injection is clearly enhanced as observed in the current onset occurring at low bias voltages. This likely reflects the energetically favourable alignment between **BDT** and MoO_3.

Summarizing the IS results for the **BDT**:$PC_{61}BM$ devices with different IFLs, a striking result is that the MoO_3 IFL containing device exhibits *no high frequency arc* (Fig. 5c and d) related to majority carrier transport limitations. In contrast, both PEDOT:PSS IFL devices exhibit the additional arc at high frequencies (Table 1 entries 6 and 7) of comparable magnitude (see R_2 in Fig. 5d). Remarkably, all three devices have the same active layer thickness and only devices having an energy level mismatch between anode workfunction and the donor molecule IP exhibit this additional resistance (Fig. 5c). The time constant of this additional process is of the same order of magnitude as that observed for recombination processes and, hence, no additional arc is observed.

Recall that the above interpretation of the IS data suggests that R_{tr} relates to hole transport while R_{rec} is determined by minority carrier electron recombination. Fig. 5d reveals that bulk transport resistance R_2 and carrier extraction at the hole selective contact are strongly correlated phenomena that also produce a large effect on recombination resistance. The actual mechanism that correlates charge extraction of holes by the IFL and transport in the bulk is not yet totally understood. However, we have previously shown for a system in which the electron collecting contact was blocked that the observed transport properties are distinctly different from those at an efficiently collecting contact.[32] Increased device thickness leads to increased R_{tr} and a reduction in R_{rec} at lower voltages than in the case of the thinnest active layer. Based on these observations we suggest that the bulk dominated transport and recombination features (R_{tr} and R_{rec}) are influenced by the charge transfer rate at the hole selective contact, as indicated schematically in Fig. 4. The failure to extract holes in the case of poor hole-selective contacts also argues that greater driving force is needed for hole transport in the blend, which is evident in the IS measurements as large R_{tr} values. In turn, this translates into a reduction in the device FF. Furthermore, while carriers generated close to the hole-selective contact can still be collected, those generated closer to the opposite selective contact are more difficult to extract and in turn decrease the recombination resistance. While in the case of the good performance MoO_3 contact, it is observed that the absence of carrier transport limitations (no second arc) also removes the pinning of the recombination resistance that displays an

exponentially decreasing behavior up to high voltage, similar to the near ideal behavior of the **P3HT**:$PC_{61}BM$ solar cell.

To emphasize the importance of energy level alignment, a different, recently published DPP derivative (**z-NDT**, Fig. 1)[20] was also examined. OPVs based on **z-NDT**:$\mathbf{PC_{61}BM}$ provide PCE of 4.3% using an optimized thickness and the IFL air-dried PEDOT:PSS (Table 1, entry 9). Surprisingly, the FF is relatively high (FF = 48%) and raises the question why in this case the same IFL that showed a reduction in FF for **BDT** shows good performance for **z-NDT**. The answer is jointly found taking into account both the **z-NDT** IP energy and the impedance spectroscopy response. A IP energy of 5.2 eV (see ESI† for CV measurements) ensures an adequate energy level matching with PEDOT:PSS dried in air. Furthermore, the impedance response shows again two arcs. Only the low frequency of arc (R_1) only decreases as V_{oc} is approached, which is the typical behavior of pure R_{rec} (Fig. 5d). Therefore, this result suggests that the PEDOT:PSS dried in air does not manifest any charge transfer impediments as otherwise R_1 would increase close to V_{oc}. Alternatively, C_1 exponentially increases as expected for well-aligned energy levels. This final result may explain why other small molecule systems found in the literature are able to provide high efficiencies using PEDOT:PSS IFLs.[8,18] However, in the **z-NDT**:$\mathbf{PC_{61}BM}$ system, the high frequency arc (R_2) related to issues of carrier transport is still present and β is low with a value of 0.30. For **z-NDT**:$\mathbf{PC_{61}BM}$ these two factors are ultimately responsible for the relatively low FF.

3. Conclusions

In this investigation of why **BDT**-based, and, by extrapolation, many other small molecule donor OPVs typically exhibit low FFs, a range of characterization techniques yields two important observations: (1) **BDT**:$PC_{61}BM$ small molecule OPV performance is severely limited by carrier transport within the bulk, and low active layer thicknesses are required to minimize recombination processes and maximize OPV performance, (2) energy level mismatches between the donor IP and the anode IFL WF also significantly limit OPV performance by suppressing hole injection from the active layer to the anode. Replacing the widely-used PEDOT:PSS IFL (WF = 5.2 eV) with MoO_3 (WF = 5.5 eV) affords a better energetic match with the **BDT** IP (5.5 eV), and the corresponding OPV FFs and PCEs are dramatically enhanced. Both phenomena are highly correlated as evidenced by impedance spectroscopy. Thus, IFL optimization should always be carried out, taking into account the donor IP energy.

Acknowledgements

We thank the following agencies for support of this research: Ministerio de Educacion y Ciencia under project HOPE CSD2007-00007, Generalitat Valenciana (ISIC/2012/008), the ANSER Center, an Energy Frontier Research Center, funded by the U.S. Department of Energy, Office of Science, Office of Basic Energy Sciences under Award Number DE-SC0001059, and the National Science Foundation through the Center for Layered Polymer Systems (CLiPS; S. L.) under grant DMR-0423914. C. J. B. acknowledges the National Science Foundation for a Graduate Research Fellowship.

Notes and references

1 M. A. Green, K. Emery, Y. Hishikawa, W. Warta and E. D. Dunlop, *Prog. Photovolt.: Res. Appl.*, 2012, **20**, 12–20.
2 G. Yu, J. Gao, J. C. Hummelen, F. Wudl and A. J. Heeger, *Science*, 1995, **270**, 1789–1791.
3 H. X. Zhou, L. Q. Yang and W. You, *Macromolecules*, 2012, **45**, 607–632.
4 P. M. Beaujuge and J. M. J. Fréchet, *J. Am. Chem. Soc.*, 2011, **133**, 20009–20029.
5 T. S. van der Poll, J. A. Love, T.-Q. Nguyen and G. C. Bazan, *Adv. Mater.*, 2012, **24**, 3646–3649.
6 K. R. Graham, P. M. Wieruszewski, R. Stalder, M. J. Hartel, J. Mei, F. So and J. R. Reynolds, *Adv. Funct. Mater.*, 2012, **22**, 4801–4813.
7 A. Mishra and P. Bäuerle, *Angew. Chem., Int. Ed.*, 2012, **51**, 2020–2067.
8 Y. Sun, G. C. Welch, W. L. Leong, C. J. Takacs, G. C. Bazan and A. J. Heeger, *Nat. Mater.*, 2012, **11**, 44–48.
9 Y. Lin, Y. Li and X. Zhan, *Chem. Soc. Rev.*, 2012, **41**, 4245–4272.
10 O. P. Lee, A. T. Yiu, P. M. Beaujuge, C. H. Woo, T. W. Holcombe, J. E. Millstone, J. D. Douglas, M. S. Chen and J. M. J. Fréchet, *Adv. Mater.*, 2011, **23**, 5359–5363.
11 B. Walker, C. Kim and T. Q. Nguyen, *Chem. Mater.*, 2011, **23**, 470–482.
12 G. Wei, X. Xiao, S. Wang, K. Sun, K. J. Bergemann, M. E. Thompson and S. R. Forrest, *ACS Nano*, 2011, **6**, 972–978.
13 H. Shang, H. Fan, Y. Liu, W. Hu, Y. Li and X. Zhan, *Adv. Mater.*, 2011, **23**, 1554–1557.
14 J. Y. Zhou, X. J. Wan, Y. S. Liu, G. K. Long, F. Wang, Z. Li, Y. Zuo, C. X. Li and Y. S. Chen, *Chem. Mater.*, 2011, **23**, 4666–4668.
15 D. Bagnis, L. Beverina, H. Huang, F. Silvestri, Y. Yao, H. Yan, G. A. Pagani, T. J. Marks and A. Facchetti, *J. Am. Chem. Soc.*, 2010, **132**, 4074–4075.
16 J. Mei, K. R. Graham, R. Stalder and J. R. Reynolds, *Org. Lett.*, 2010, **12**, 660–663.
17 F. Silvestri, M. D. Irwin, L. Beverina, A. Facchetti, G. A. Pagani and T. J. Marks, *J. Am. Chem. Soc.*, 2008, **130**, 17640–17641.
18 J. Zhou, X. Wan, Y. Liu, Y. Zuo, Z. Li, G. He, G. Long, W. Ni, C. Li, X. Su and Y. Chen, *J. Am. Chem. Soc.*, 2012, **134**, 16345–16351.
19 G. Li, V. Shrotriya, J. Huang, Y. Yao, T. Moriarty, K. Emery and Y. Yang, *Nat. Mater.*, 2005, **4**, 864–868.
20 S. Loser, H. Miyauchi, J. W. Hennek, J. Smith, C. Huang, A. Facchetti and T. J. Marks, *Chem. Commun.*, 2012, **48**, 8511–8513.
21 S. Loser, C. J. Bruns, H. Miyauchi, R. P. Ortiz, A. Facchetti, S. I. Stupp and T. J. Marks, *J. Am. Chem. Soc.*, 2011, **133**, 8142–8145.

22 A. Guerrero, L. F. Marchesi, P. P. Boix, J. Bisquert and G. Garcia-Belmonte, *J. Phys. Chem. Lett.*, 2012, **3**, 1386–1392.
23 P. P. Boix, A. Guerrero, L. F. Marchesi, G. Garcia-Belmonte and J. Bisquert, *Adv. Energy Mater.*, 2011, **1**, 1073–1078.
24 G. Garcia-Belmonte, A. Guerrero and J. Bisquert, *J. Phys. Chem. Lett.*, 2013, **4**, 877–886.
25 F. Fabregat-Santiago, G. Garcia-Belmonte, I. Mora-Seró and J. Bisquert, *Phys. Chem. Chem. Phys.*, 2011, **13**, 9083–9118.
26 J. Bisquert and G. Garcia-Belmonte, *J. Phys. Chem. Lett.*, 2011, **2**, 1950–1964.
27 S. R. Cowan, N. Banerji, W. L. Leong and A. J. Heeger, *Adv. Funct. Mater.*, 2012, **22**, 1116–1128.
28 D. Credgington, F. C. Jamieson, B. Walker, T.-Q. Nguyen and J. R. Durrant, *Adv. Mater.*, 2012, **24**, 2135–2141.
29 Z. M. Beiley, E. T. Hoke, R. Noriega, J. Dacuña, G. F. Burkhard, J. A. Bartelt, A. Salleo, M. F. Toney and M. D. McGehee, *Adv. Energy Mater.*, 2011, **1**, 954–962.
30 P. P. Boix, Y. H. Lee, F. Fabregat-Santiago, S. H. Im, I. Mora-Sero, J. Bisquert and S. I. Seok, *ACS Nano*, 2011, **6**, 873–880.
31 Y. Zhang, X.-D. Dang, C. Kim and T.-Q. Nguyen, *Adv. Energy Mater.*, 2011, **1**, 610–617.
32 T. Ripolles-Sanchis, A. Guerrero, J. Bisquert and G. Garcia-Belmonte, *J. Phys. Chem. C*, 2012, **116**, 16925–16933.
33 A. Guerrero, T. Ripolles-Sanchis, P. P. Boix and G. Garcia-Belmonte, *Org. Electron.*, 2012, **13**, 2326–2332.
34 J. Bisquert and I. Mora-Seró, *J. Phys. Chem. Lett.*, 2009, **1**, 450–456.
35 A. Garcia, G. C. Welch, E. L. Ratcliff, D. S. Ginley, G. C. Bazan and D. C. Olson, *Adv. Mater.*, 2012, **24**, 5368–5373.
36 E. L. Ratcliff, J. Meyer, K. X. Steirer, N. R. Armstrong, D. Olson and A. Kahn, *Org. Electron.*, 2012, **13**, 744–749.
37 M. D. Irwin, J. D. Servaites, D. B. Buchholz, B. J. Leever, J. Liu, J. D. Emery, M. Zhang, J.-H. Song, M. F. Durstock, A. J. Freeman, M. J. Bedzyk, M. C. Hersam, R. P. H. Chang, M. A. Ratner and T. J. Marks, *Chem. Mater.*, 2011, **23**, 2218–2226.
38 R. Po, C. Carbonera, A. Bernardia and N. Camaioni, *Energy Environ. Sci.*, 2011, **4**, 285–310.
39 R. Steim, F. R. Kogler and C. J. Brabec, *J. Chem. Mater.*, 2010, **20**, 2499–2512.
40 J. D. Servaites, M. A. Ratner and T. J. Marks, *Energy Environ. Sci.*, 2011, **4**, 4410–4422.
41 J. D. Servaites, S. Yeganeh, T. J. Marks and M. A. Ratner, *Adv. Funct. Mater.*, 2010, **20**, 97–104.
42 M. Y. Chan, C. S. Lee, S. L. Lai, M. K. Fung, F. L. Wong, H. Y. Sun, K. M. Lau and S. T. Lee, *J. Appl. Phys.*, 2006, **100**, 094506.
43 H. Frohne, S. E. Shaheen, C. J. Brabec, D. C. Müller, N. S. Sariciftci and K. Meerholz, *ChemPhysChem*, 2002, **3**, 795–799.
44 J. Huang, P. F. Miller, J. S. Wilson, A. J. de Mello, J. C. de Mello and D. D. C. Bradley, *Adv. Funct. Mater.*, 2005, **15**, 290–296.
45 Y. Sun, C. J. Takacs, S. R. Cowan, J. H. Seo, X. Gong, A. Roy and A. J. Heeger, *Adv. Mater.*, 2011, **23**, 2226–2230.
46 J. Meyer, A. Shu, M. Kroger and A. Kahn, *Appl. Phys. Lett.*, 2010, **96**, 133308.